Digitally Reconfigurable Metasurface Array for A Multipath Based Wireless Link with Media-Based Modulation

Aritra Roy, *Student Member, IEEE*, Yalagala Naresh, Ashwin Padmanabhan, *Member, IEEE*
Ananthanarayanan Chockalingam, *Senior Member, IEEE* and K J Vinoy, *Senior Member, IEEE*

***Abstract*—Electromagnetic windows with a digitally reconfigurable metasurface (DRM) is proposed to experimentally demonstrate a multipath based communication technique known as media-based modulation (MBM). In MBM, the magnitude and phase of a transmitted tone from a single RF chain is modulated in space using different switching combinations of DRM. After transmission, superposition of various multipath components help diversifying the transmitted symbols across the constellation leading to an improved signal-to-noise ratio (SNR), bandwidth and energy efficient multiuser system with enhanced security, reduced outage probability in a slow fade channel and possibility of achieving capacity of a Gaussian channel. Prototype of an 8×8 array of the DRM unit cells with PIN diodes for switching, and its hardware interface are developed to perform experiments under different scattering environments. Constellations, BER (bit-error-rate) responses and statistical distributions of the received symbols with the measured data establish the above characteristic features of a wireless link using MBM. A scheme for the data transmission with DRM is also discussed.**

***Index Terms*—Digitally reconfigurable metasurface, media-based modulation, scatter-rich environment, channel fade coefficients.**

I. Introduction

Multipath components in a practical communication channel are considered as one of the serious bottlenecks that limits the performance of a wireless link. Signals traveling through multiple paths experience different magnitude and phase modifications causing fading which can even lead to a transmission outage. In a slow fade channel a transmission outage can only be overcome by waiting till the channel response is improved or by reducing the data rate. Techniques such as space shift keying (SSK), spatial modulation (SM), generalized spatial modulation (GSM), multiple input and multiple output (MIMO) [1]–[3], massive MIMO [4], ultra massive MIMO [5]. are often employed to address multiple users simultaneously. Here, multipath propagation is addressed with spatial diversity by sending the same signal from different spatial locations with multiple antennas. In these systems, the signals from different antennas are considered to be different channel realizations resulting in different complex received powers. Channel fading augments the Euclidean distances among these transmitted spatial signatures making the received magnitudes and phases (received symbols) easily detectable to the receiver and improves the bit rate (spectral efficiency), bit-error-rate (BER) and mutual information of a wireless link [1]. SSK utilizes N antennas to transmit N symbols by turning on one antenna at a time. Antennas are usually placed $\lambda/2$ from each other that makes the overall transmitter large. To reduce this hardware burden, innovative approaches such as electronically steerable parasitic arrays [6], near field direct antenna modulation [7], [8], load modulated array [9], pattern reconfigurable array [10], [11], mode shift keying [12] have been attempted. MIMO systems adopt a beamsteering or beamforming based approach with antennas surrounded by either parasitic antennas or structures to achieve these goals [13], [14].

Media based modulation (MBM) uses a single antenna to replicate the functionality of a multiantenna system where reconfigurable electromagnetic structures close to an antenna are switched to modulate the magnitude and phase of the transmitted tone to generate different spatial signatures (transmitting symbols) as explained in Fig. 1. The RF chain is simplified as this scheme needs only one transmitting antenna compared to an SSK or a MIMO [1]. These digitally reconfigurable (ON-OFF) unit cells can be designed with sub wavelength dimensions to make the overall structure compact. The spectral efficiency can be improved at a linear rate (with respect to number of reconfigurable unit cells) in MBM. In addition, MBM is a powerful multiuser system saving the transmission bandwidth and energy [15] providing high security in the physical layer [16]. Since the spatial signatures (which are analogous to controlled channel conditions) are generated with an intentional switching of EM windows in MBM, the effect of bad channel condition does not prevail and both good and bad channel conditions contribute in the cardinality of the constellation (diversifying symbols across constellation). The transmission outage in a slow fade channel can be overcome without sacrificing the transmission rate. This phenomenon with a large constellation essentially converts a static multipath fading channel into a non-fade AWGN channel achieving its capacity [17]. More features, advantages and other technical aspects of MBM are discussed in [15]–[19]. However, no experimental validation of MBM has been reported so far to demonstrate its key advantages in exploiting multipath

Authors are with the Department of Electrical Communication Engineering, Indian Institute of Science, Bangalore, Karnataka, 560012, India. e-mail: (aritra@iisc.ac.in).

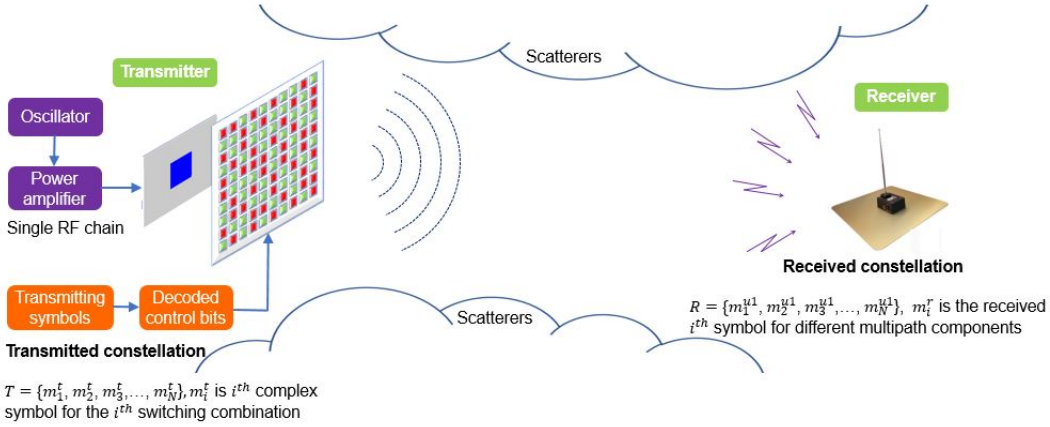

Fig. 1. MBM transmitter consisting of a digitally reconfigurable metasurface in front of a transmitting antenna with single RF chain. The receiver picks up different multipath components. The receiving constellation R is the vector sum of the corresponding multipath components. Performance of MBM is relatively poor in an ideal free-space environment and improves in the presence of scatterers.

propagation and its inherent channel diversity over a static fading channel, though a similar hardware that proves the innate communication system security aspect alone has been presented in [16]–[18].

In the proposed work, a compact prototype of MBM modulator consisting of a digitally reconfigurable metasurface (DRM) and a patch antenna is designed and characterised. The metasurface as a 2D equivalent of the metamaterials [20] have been extensively used for different microwave applications such as antenna performance improvement [21], [22], electronic tuning [23], [24], multibeam generation [25], RCS reduction [26], electromagnetic imaging [27] and even for MIMO and other wireless applications [28]–[30]. Recently, large programmable metasurfaces are proposed to implement wireless systems with a single RF chain [31]–[35]. These techniques experimentally demonstrated efficient transmission of information over wireless channels introducing several new techniques such as frequency and space division multiplexing [31], space down conversion [35] etc. But in general, multipaths are considered as an undesired phenomena, and communication systems have been developed for overcoming their effects. Although intelligent reflecting surfaces [36], [37] engineer multipath components to communicate in NLOS environments, approaches for their implementation are still evolving.

In the scheme experimentally proposed here, a single antenna is shown to provide the performance of a multi-antenna system [38]. The tone from this antenna is spatially modulated by the switching combinations of the array. In Sec. II, the design of metasurface and DRM modulator are discussed with extended EM simulations. The fabricated prototype with measured data under different scattering environments including an extension for a multiuser system exploiting the channel behaviour are presented in Sec. III. A brief demonstration of data transmission with DRM in Sec. IV. is followed by the conclusion in Sec. V.

II. Design of DRM based Modulator

In this work, a DRM is proposed to design a modulator for MBM. A PIN diode is used in the unit cell of DRM to make it reconfigurable. In this section, the design of this unit cell, DRM array and its control are discussed.

A. DRM Unit Cell

Schematic of the DRM unit cell is shown in Fig. 2(a), with overall dimension 10×10 mm^2 making it $\lambda_0/7.5$ in size where, λ_0 is the free space wavelength at the design frequency of 4 GHz [39]. This unit cell has a planar beam-Lead PIN Diode (DSG9500-000, Skyworks Solutions, Inc.) for switching between two distinct states of different transmission characteristics. Dimensions used in this design ($w_m = 7.1$ mm, $l_m = 5.59$ mm, $s_m = 1$ mm, $g_m = 0.53$ mm, $w_{st} = 1$ mm, $g_{mst} = 2$ mm and $g_u = 0.2$ mm) produce transmission zeros at 4 GHz and at 5.3 GHz when the diode is turned ON and OFF respectively. The unit cell has a high inductance due the unfurled length [40], [41] making it more compact compared to a previous work [42]. The gap between traces account for the capacitance required to make the unit cell resonate at the desired frequency. A three-turn meander is placed at the center with two horizontal strips on an FR-4 (ε_r = 4.3, tanδ = 0.025) substrate of thicknesses 0.5 mm. The electromagnetic windowing operation is achieved by reconfiguring the surface impedance of the unit cell with digital inputs from a controller. The control signal trace is printed at the opposite side of the substrate and connected to the meander through a via. The top horizontal strip is used as the common ground for the diode.

CST Microwave Studio is used to design the unit cell with the objective to obtain sufficient difference between the transmitted powers of the two distinct switching states. Simulated $|S_{21}|$ of the unit cell for ON and OFF states are shown in Fig. 2(b), where the effects of incorporating the biasing lines are also depicted. When the transmission zero is at 4 GHz, the $|S_{21}|$ is -20.8 dB making the unit cell

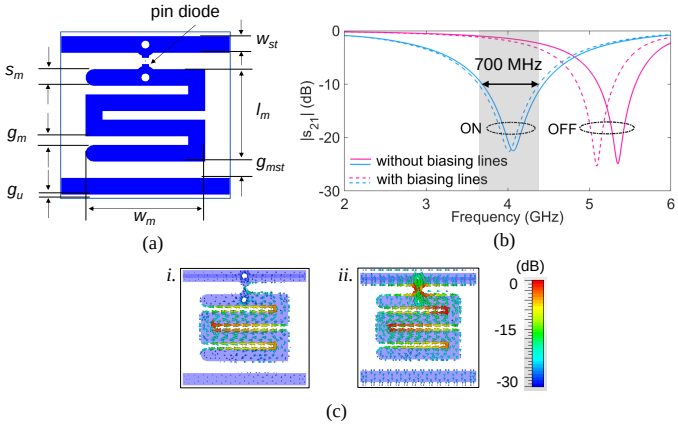

Fig. 2. (a) Schematic of the proposed metasurface unit cell, (b) Simulated $|S_{21}|$ of the unit cell at different switching conditions with and without the biasing lines, (c) Normalized surface current distributions at *i.* 5.3 GHz and *ii.* 4 GHz

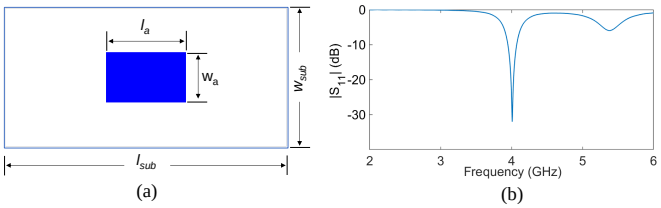

Fig. 3. (a) Schematic of the patch antenna, (b) simulated $|S_{11}|$ of the antenna

blocking the transmitted signals. When the diode is turned OFF, the transmission zero is shifted to 5.3 GHz and the $|S_{21}|$ at 4 GHz becomes -1.5 dB and the unit cell is considered as *transmitting*. The difference in the transmitted powers of the unit cell is found to be more than 10 dB over a band of 700 MHz. The normalized surface current distributions at the resonant frequencies in Fig. 2(c) gives more physical insight to the operation of the unit cell in the two states. In the *transmitting* state, the current is restricted to the meander alone as the diode is OFF. In the other state, the current is distributed over the meander as well as the horizontal strip above. Hence, the longer current path and lower resonant frequency is observed in the latter state.

B. Transmitting Antenna

Since the concept of MBM requires only a single tone to be transmitted, a simple probe fed rectangular microstrip patch antenna is used in this work as shown in Fig. 3(a). The patch dimensions are: $l_a = 34$ mm and $w_a = 21.85$ mm to operate at a frequency of 4 GHz as shown in Fig. 3(b). An Arlon AD-250 substrate (ε_r = 2.5, tanδ = 0.0018) with a thickness of 1.57 mm is used. The overall dimension of the dielectric slab is kept $l_{sub} = 120$ mm and $w_{sub} = 60$ mm to align with the metasurface screen dimensions.

C. Proposed Modulator with DRM

MBM transmitter shown in Fig. 1 uses different sets of unit cells to modulate a transmitting tone to generate different transmitting symbols (magnitude and phase). The MBM transmitter is designed by extensive EM simulations using CST Microwave Studio. The unit cells designed above are arranged as a planar array in front of the patch and the field radiated at boresight is simulated by switching the unit cells between *transmitting* and *blocking* states. For an array with $n \times n$ unit cells, 2^{n^2} switching states are possible leading to as many complex field values, which may be used as constellation points for this transmitter. Since the array is in the nearfield of the antenna, these constellation points vary with the distance of the array and the antenna. In some cases, the loading effect of the array may affect the impedance characteristics and deteriorates the antenna matching. It has been observed that a small array may have less impact on the antenna performance but has fewer options for constellation points. On the other hand, a large array can produce more points, but with less parasitic effects. Therefore a compromise is needed on the interaction between the antenna and the array to design the transmitter with a larger spread of constellation points at a given observation point. Therefore parametric studies are conducted by changing the array size and its distance from the antenna to arrive at their optimum values.

In the first simulation study, the magnitudes (field values at boresight) corresponding to all unit cells of the array in their *transmitting* (all ON) and *blocking* (all OFF) states are analyzed. In Fig 4(a), the blue bars indicate the magnitudes of field values for different array sizes in their *transmitting* states. This is found to be maximum for the 8×8 array size. The normalization of magnitudes for other arrays are performed by setting the global maximum of 8×8 array as the reference. In the same figure, green bars indicate the difference between the field magnitudes between the *transmitting* and *blocking* states (ΔMagnitude) for different array sizes. It is observed that ΔMagnitude increases with the array size as the aperture of blocking increases too. Although the hardware complexity increases with a larger array, this would facilitate a better MBM implementation by generating a higher number of constellation points. Therefore, an 8×8 array is considered for the DRM in the present investigation.

The above mentioned studies are performed by keeping a distance of 40 mm between the DRM and antenna. Interactions between the unit cells of array and the patch antenna affect the impedance matching of the later for certain switching combinations. To study this phenomena, the metasurface is kept at different distances away from the antenna and the total number of switching combinations below different $|S_{11}|$ levels are summarised in Fig. 4(b). It is seen that good matching ($|S_{11}| < -10$dB) is observed for maximum number of cases with a gap of 40 mm. It may be noted that this spacing is close to $\lambda/2$ at 4 GHz and is also consistent with the observations in [43]. In this study we restricted the analysis to 2^8 distinct cases by switching all elements in one column of the array, together. Since only 26 switching states are worse than the -10 dB threshold, 8×8 array kept at 40 mm from the antenna is used for further investigations.

It may be noted that if individual unit cells are separately

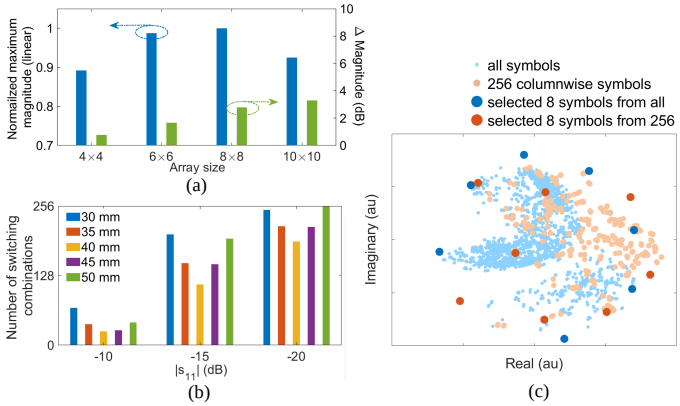

Fig. 4. (a) Normalized maximum farfield magnitude and ΔMagnitude for different array sizes, (b) Number of switching combinations for which the $|S_{11}|$ are below below different amplitude levels for different antenna-DRM distances, (c) All symbols and selected symbols from the constellation for different switching and columnwise switching.

TABLE I
MINIMUM EUCLIDEAN DISTANCES

	2 symbol	4 symbols	8 symbols
all symbols	0.70	0.42	0.19
256 symbols for coulmnwise control	0.65	0.41	0.18

controlled, a total of 2^{64} (18×10^{18}) switching combinations and as many symbols are possible to obtain. However in practical applications such a large number may become impractical. A comparison of distribution of constellation points is shown in Fig. 4(c) where we attempted to increase the number of possibilities by choosing different sets of unit cells. The real and imaginary parts of the complex field values at boresight are plotted here as constellation points. The increase in the spread in Fig. 4(c) is found to be marginal when other possible switching combinations are appended with the columnwise control. Now, in a practical system, only a few symbols are required for data communications (2, 4 or 8 in cases are studied below) with the minimum Euclidean distance among them maximised. Therefore, a comparison of Euclidean distances after selecting these 2, 4, and 8 symbols from sets of 256 (columnwise) and 2048 (all considered) constellation points are included in Table I, that shows the minimum Euclidean distance does not increase significantly even if smaller group of unit cells are controlled separately. On the other hand, controlling individual unit cells separately, increases the hardware complexity significantly. Hence the DRM and its controller are designed to control each column of the array as one unit, resulting in a maximum of 2^8 constellation points.

PIN diodes in unit cells is controlled using an Arduino microcontroller interfaced to a Laptop. These diodes draw a current of up to 15 mA when turned ON. Since eight diodes

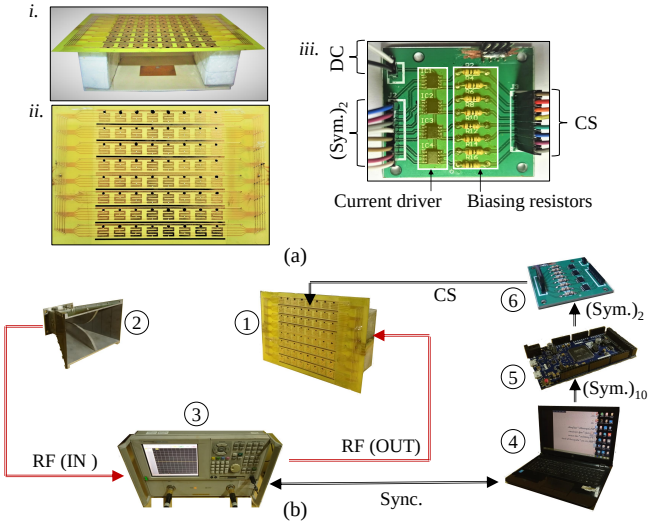

Fig. 5. (a) Fabricated prototype of *i.* DRM and antenna, *ii.* DRM array and *iii.* current driver circuit. (b) The underlying system for measurement with ① DRM modulator, ② horn, ③ VNA, ④ interface generating synchronism signal (Sync.) and symbols in decimal ($(Sym.)_{10}$), ⑤ Adruino generating the binary equivalence of symbols ($(Sym.)_2$), ⑥ driving circuit generating control signals (CS)

are connected in parallel in one column, a MoSFET based high speed current driver (IXDN602SIA) with current limiting resistors are used for its control. This driver circuit has eight separate connections to the DRM.

III. EXPERIMENTAL VERIFICATION

A. Fabricated Prototype

A prototype of the reconfigurable metasurface structure is fabricated and shown in Fig. 5(a)*i.* and *ii.*. The 8×8 array is printed on one side of the substrate where the control lines are patterned on the other side. The fabricated prototype of the current driving circuit with the inputs (*binary symbols from Adruino* ($Sym._2$)), outputs (CS. *control signal to the array*) are shown in Fig. 5(a)*iii*.

A schematic of the measurement setup is shown in Fig. 5(b). A python interface generates the symbols to be transmitted ($Sym._{10}$) that are fed to an Adruino micro-controller board that generates the decoded eight bit data ($Sym._2$) corresponding to the input symbol. The current driver circuit produces the required currents (CS) for the diodes in the metasurface array according to the Adruino output. A 4 GHz tone is transmitted by the antenna assembly and is received by the receiving horn and the S_{21} is continuously measured by a Keysight N5230A PNA Series vector network analyzer. The VNA is interfaced with the laptop to download the data, to synchronise (Sync.) the entire process from symbol generation to data acquisition.

A schematic of measurement arrangement inside and outside anechoic chamber in different configurations are shown in Fig. 6(a). Similar measurements are also performed in the laboratory environment with scattering objects such as chairs, tables, storage shelves and exposed walls (scatter-rich channel).

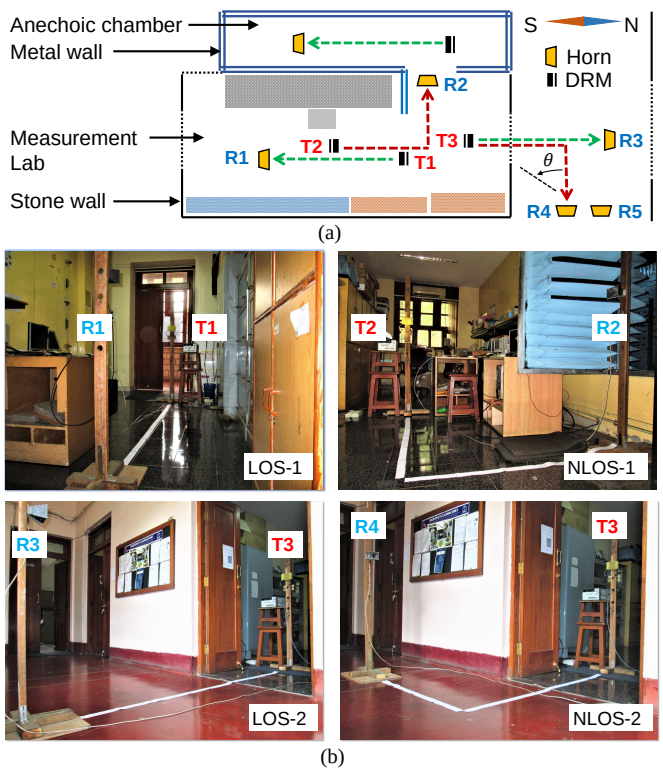

Fig. 6. (a) Schematic of measurement arrangements inside and outside the anechoic chamber, (b) Photograph of measurement arrangement in LOS and NLOS configurations.

B. Performance in Scatter-free and Scatter-rich Channels

Exploitation of multipath fading is one of the major features of MBM scheme. To analyze the effects of multipath on the wireless link, contellations for selected switching states are measured inside and outside the anechoic chamber with the modulator facing the receiving horn antenna in an LOS configuration. The observed field values are spatial signatures embedded by the metasurface to the transmitted tone. These cases are repeated with different distances between the transmitter-receiver pair by placing the transmitter on a rack and pinion arrangement atop a mast. This arrangement allowed movement of the transmitter by turning a screw. For clarity, constellations of ten states for four different screw positions (moving the transmitter by around $\lambda/4$ successively) inside the chamber are plotted in Fig. 7(a). The rotation (by 90^0) of centroids of these clusters is clearly visible. The magnitude variation among these clusters is marginal as the overall distance between the antennas are very close to one another.

An identical set of switching states are evaluated outside the anechoic chamber at similar distances in a scattering environment depicted in Fig. 6(a). Resulting constellations are compiled in Fig. 7(b) where no distinct clusters are observed unlike the previous case. However, these contellation points are distributed over an annular region. It is clear that multipath components affect both amplitude and phase corresponding to

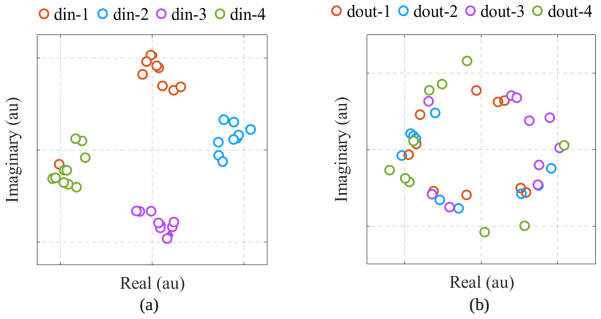

Fig. 7. Measured constellations for different switching combinations (a) inside and (b) outside the anechoic chamber

each point. These are significantly dispersed due to the random scattering environment. It may be noted that the received field values are the superposition of the spatial signatures received directly as well as by multipath components from the surrounding scatterers.

C. Studies in Multipath Environments

Having the established fact that constellation points are more spread out in a scattering environment, the above laboratory experiments are extended for different configurations to evaluate the performances in different multipath environments. These include cases with and without a direct paths (LOS and NLOS) of propagation between antennas. as shown in Fig. 6(a). Our laboratory consists of cupboards, tables, chairs, and other scatterers of different sizes, shapes and materials in addition to doors and windows with a granite stone walls on three sides and a shielded anechoic chamber on the fourth. Reinforced cement concrete slabs form top and bottom surfaces of the laboratory. The transmitter and the horn antenna are placed at different pairs of locations in this laboratory environment to evaluate the performance of the MBM transmitter in different LOS and NLOS scenarios. Accordingly, referring to Fig. 6(a) the following configurations are attempted: (a) LOS-1 (R1-T1): both transmitter and receiver within the lab, (b) LOS-2 (R2-T2): transmitter inside and receiver directly outside the door, (c) NLOS-1 (R3-T3): transmitter and receiver inside the lab with a shielded surface blocking the line of sight, and (d) NLOS-2 (R4-T3): transmitter inside and receiver outside the lab with a stone wall blocking each other. Photograph of these configurations with transmitter and receiver are shown in Fig. 6(b).

Constellations for these LOS and NLOS configurations are summarized in Fig. 8(a)*i.*, *ii.* and Fig. 8(b)*i.*, *ii.*, respectively. Despite the identical transmission in each configuration, the scatter is different in these cases, indicating diverseness of multipath components in these arrangements. Due to the absence of any direct path, the received power are significantly reduced in NLOS configurations. From each scatterplot with 64 constellation points, a Euclidean distance measure can be used to identify 2 or 4 symbols for communication [1]. These symbols are selected using a search algorithm that maximizes the minimum Euclidean distance among them.

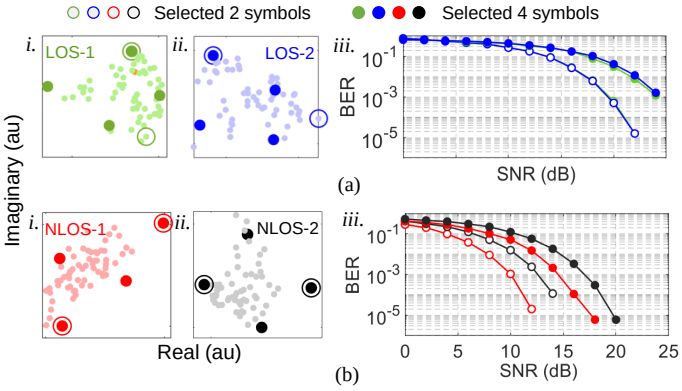

Fig. 8. Measured (a) constellations for *i.* LOS-1, *ii.* LOS-2 and *iii.* BER response for LOS configurations. Measured (b) constellations for *i.* NLOS-1, *ii.* NLOS-2 and *iii.* BER response for NLOS configurations.

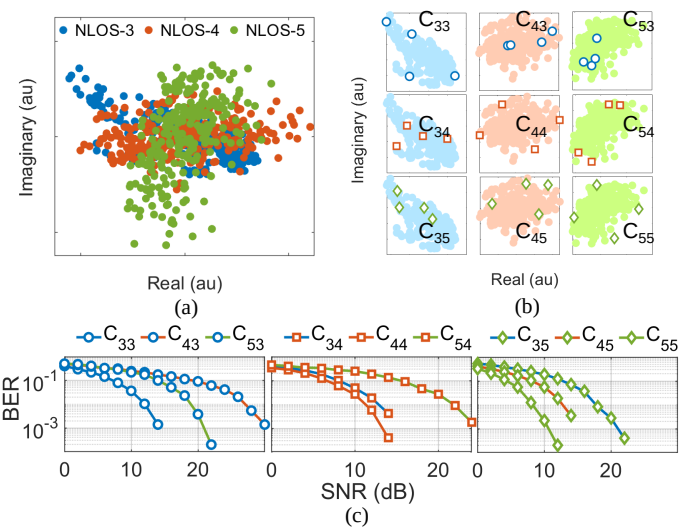

Fig. 9. (a) Measured constellations for NLOS-3, NLOS-4 and NLOS-5 after normalization, (b) Location of best selected symbols from NLOS-3, NLOS-4 and NLOS-5 and the location of those on other constellations, (c) BER response of the best selected symbols from NLOS-3, NLOS-4 and NLOS-5 compared to the same on other constellations

The calculated BER performances of these LOS and NLOS configurations are plotted in Fig. 8(a)*iii.* and Fig. 8(b)*iii.*, respectively. For all the four cases, SNR requirements for 2 symbols are less than those for the 4 symbols. This relationship is straight forward and well established as selecting more symbols from a fixed scatter effectively reduces the Euclidean distances among the symbols, leading to degraded error rates for fixed SNRs. From Fig. 8(a)*iii.*, it is observed that the error rates for LOS-1 and LOS-2 are nearly overlapped. As the direct path powers are significantly more than the multipath powers, the LOS is unable to augment the Euclidean distances among the symbols even though scatterers are present. On the other hand, Fig. 8(b)*iii.* show significant improvements in the error rates as the symbols are augmented well across the constellation. For example, in a 2 symbol case LOS-1 and LOS-2 require around 20 dB of SNR for the BER of 10^{-3}, whereas the same with NLOS-1 is only 10 dB. This implies that the same error rate is achieved in NLOS with reduced transmit power by utilising the multipath components. These measurements confirm the numerical predictions of performance improvement in MBM when scatterers are present [1], [15], [18]. To reduce the number of experimental cases, the outer columns of the DRM are kept in the *transmit* case to generate the above scatterplot measurements. It must be recalled that communication in NLOS arrangements depend primarily on signal components reflected from the surroundings.

It may be noted that since transmitting symbols are encoded as control sequences which operate switches in the array to embed different spatial signatures to this tone, it is clear that this system will not be impacted by nonlinearity of the power amplifier and hence the overall efficiency of the MBM transmitter can be high.

D. Security for Multiple Users

The experimental scenarios investigated above had single transmitter and receiver. In this section features of MBM for a multiuser system in a static scatter-rich environment are investigated. Three sets of NLOS scatterplots are measured in the environment shown in Fig. 6(a), where the modulator is kept fixed at T3 and the receiving horn is placed at different locations (R4 looking west, R4 looking southwest, and R5 looking west). These are named NLOS-3 to -5 in this figure. The measured constellations for these scenarios consisting of 256 (2^8) points each, are shown in Fig. 9(a) after normalization to zero mean and unit variance. These show significant differences among them, even though the scattering environment remain static. A unique set of four symbols can be identified based on Euclidean distance measure, from each of these sets of measurements. These sets of symbols are unique to the measurement scenario as illustrated in Fig. 9(b). For example, if we identify the symbols from the measurement NLOS-3, positions of these symbols in the complex plane (in C-33) change with the measurement scenario, as indicated by C-43 and C-53 of Fig. 9(b) for NLOS-4 and NLOS-5, respectively. Similarly, the second row of Fig. 9(b) show deviations observed for symbols identified from NLOS-4 in the other two scenarios. The randomness of deviations are observed in the third case as well. The impact of these deviations are quantified in the BER plot in Fig. 9(c) which shows that performance achieved degrade as the scenario is changed. It is clear that the minimum Euclidean distance within the set of four symbols indicate the SNR of the MBM system and is the highest for the set of symbols corresponding to that constellation. Since the switching states corresponding to the set of symbols in each of these measurement sets are uncorrelated, receivers at these positions can function independently with different codebooks.

As noted from the above, significant variation of the received symbols are observed due to strong multipath components even for small changes in the receiver locations. Apart from the benefits of multiple received codebooks with multipath components, MBM offers an enhanced security to

the wireless link [16] by spatial coding. Users only at a certain spatial location can decode the symbols belonging to his codebook being oblivious about the messages of the neighbours and vice versa. This ensures an enhanced physical layer security embedded in the wireless link by the multipath components in the scatter rich environments used for MBM. Here, the received complex vector of length D represents D parallel channels mimicking the behavior of a $D \times D$ MIMO-SBM system. In other words, D different messages can be received in a single transmission using the same transmitted energy and bandwidth, leading to "D times energy harvesting" [15]. In contrast, in a conventional SIMO-SBM (single input and multiple output-source based modulation) system with D receivers, the received vector of length D indicates a single complex point in the constellation.

E. Rayleigh to Gaussian Channel Conversion in MBM

For a conventional SBM, the effect of a low gain channel can be severe and transmission outage can happen indefinitely for a slow fade channel. In SBM, this outage can only be overcome by reducing the rate of transmission or by waiting till the channel condition improves. On the other hand, the channel realizations (spatial signatures) in MBM are controlled by DRM, where both good and bad channels may contribute to the cardinality of the constellation. Hence it may be possible to alleviate transmission outages without sacrificing the transmission rate or the spectral efficiency.

To investigate this feature of MBM with a large constellation, experiments are performed under different NLOS environments by placing the transmitter and receiver at dozens of random locations in the Laboratory environment in different orientations ensuring no direct path between them. All sets of scatterpoints are normalized to zero mean and unit variance and are plotted in Fig. 10(a). Here, the near and far points from the center indicate low and high power levels of the symbols, respectively. The real and imaginary components of these are plotted separately in Fig. 10(b) *i.* and *ii.*, respectively. It can be observed that both real and imaginary components are Gaussian distributed, thereby proving the conversion of a fading channel into an AWGN channel [18]. Therefore, MBM can achieve the capacity of a non-fade Gaussian channel as it effectively utilizes many multipath components for communication. In other words, the scatterers help diversifying the received symbols across the constellation to help the wireless link overcome poor channel conditions (such as a slow fade channel) without sacrificing the spectral efficiency of the system [18]. For larger constellations, these channel realizations can asymptotically convert a static fading channel into an Gaussian (Ergodic) channel.

IV. Data Transmission with DRM

An experiment for data transmission was performed in a laboratory environment where a text message is transmitted and received with MBM. The DRM is used as transmitter and a horn antenna in an NLOS configuration is used as the receiver. A program with a graphical user interface was

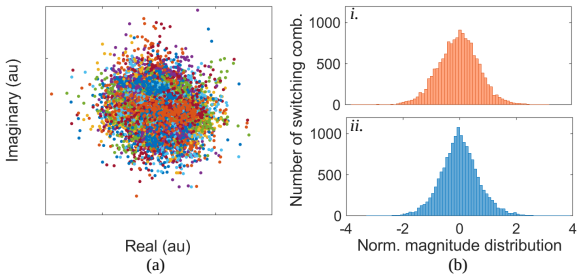

Fig. 10. (a) Measured constellations consisting of 14,848 symbols after normalization and (b) their distribution of *i.* real and *ii.* imaginary components.

developed to conduct this experiment to transmit and receive the data from a laptop. Atfirst the DRM is operated for 256 switching cases and the complex S_{21} was recorded using a VNA. The Euclidean distance measure based algorithm was used to identify the required number of symbols from these constellation points for the data transmission. After this calibration step, the data is transmitted by keeping channel states static. A text message to be transmitted is converted into ASCII and are split into suitable number of bits depending on the number of symbols and the corresponding DRM states are used to transmit them. At the receiver, the complex data was mapped to the pre-selected symbols using a k-means clustering algorithm. Based on the decoded data, ASCIIs and hence the actual transmitted text was generated at the receiver [44].

V. Conclusion

In this work, an implementation of a compact media based modulation (MBM) transmitter using a digitally reconfigurable metasurface (DRM) in the near-field of a microstrip patch antenna and the experimental studies of its performance in a multipath environment are presented. The metasurface is designed with unit cells of meandered line and a PIN diode for reconfiguring its transmission performance. The spatial signatures generated by the modulator and the multipath propagation components contribute to the improvement of the wireless link. Unlike beam forming techniques using a similar antenna-DRM arrangement, the operation of an MBM transmitter is very unique [18]. Since the multipath components are non-deterministic, the performance of the proposed modulator is evaluated inside an anechoic chamber and in various scenarios in a laboratory environment at different positions. Using the measured constellations (received complex fields) it is shown that the changes (for different switching conditions at different distances) in magnitudes and phases are consistent with distance if there is no multipath component in the environment. The same experiment repeated in a scattering environment with multipath demonstrated the randomness in the arrangement of received field values. Experiments in LOS and NLOS configurations under scatter-rich environments are used to evaluate the corresponding constellation and bit error rate diagrams. These measurements demonstrated that the error rate is significantly improved when multipath components are significant. The possibility of MBM in a multiuser scenario

is also investigated experimentally. It is shown that using a single transmission, multiple users can receive different messages without increasing the bandwidth or the transmitted power. Possibility of an enhanced security of the wireless link by MBM is also discussed. A large constellation of measured symbols in different NLOS arrangements is used to demonstrate that the symbols are Gaussian distributed, thereby proving the ability of MBM to convert a static fading channel into a non-fading AWGN channel. A demonstration of data transmission in a scatter rich laboratory environment is also presented.

REFERENCES

[1] Y. Naresh and A. Chockalingam, "On media-based modulation using rf mirrors," *IEEE Transactions on Vehicular Technology*, vol. 66, no. 6, pp. 4967–4983, 2017.

[2] M. D. Renzo, H. Haas, and P. M. Grant, "Spatial modulation for multiple-antenna wireless systems: a survey," *IEEE Communications Magazine*, vol. 49, no. 12, pp. 182–191, 2011.

[3] M. Di Renzo, H. Haas, A. Ghrayeb, S. Sugiura, and L. Hanzo, "Spatial modulation for generalized mimo: Challenges, opportunities, and implementation," *Proceedings of the IEEE*, vol. 102, no. 1, pp. 56–103, 2014.

[4] A. Amiri, M. Angjelichinoski, E. de Carvalho, and R. W. Heath, "Extremely large aperture massive mimo: Low complexity receiver architectures," in *2018 IEEE Globecom Workshops (GC Wkshps)*, 2018, pp. 1–6.

[5] C. Han, J. M. Jornet, and I. Akyildiz, "Ultra-massive mimo channel modeling for graphene-enabled terahertz-band communications," in *2018 IEEE 87th Vehicular Technology Conference (VTC Spring)*, 2018, pp. 1–5.

[6] K. Gyoda and T. Ohira, "Design of electronically steerable passive array radiator (espar) antennas," in *IEEE Antennas and Propagation Society International Symposium. Transmitting Waves of Progress to the Next Millennium. 2000 Digest. Held in conjunction with: USNC/URSI National Radio Science Meeting (C*, vol. 2, 2000, pp. 922–925 vol.2.

[7] A. Babakhani, D. B. Rutledge, and A. Hajimiri, "Transmitter architectures based on near-field direct antenna modulation," *IEEE Journal of Solid-State Circuits*, vol. 43, no. 12, pp. 2674–2692, 2008.

[8] ——, "Near-field direct antenna modulation," *IEEE Microwave Magazine*, vol. 10, no. 1, pp. 36–46, 2009.

[9] M. A. Sedaghat, V. I. Barousis, R. R. Müller, and C. B. Papadias, "Load modulated arrays: a low-complexity antenna," *IEEE Communications Magazine*, vol. 54, no. 3, pp. 46–52, 2016.

[10] Z. Li, D. Rodrigo, L. Jofre, and B. A. Cetiner, "A new class of antenna array with a reconfigurable element factor," *IEEE Transactions on Antennas and Propagation*, vol. 61, no. 4, pp. 1947–1955, 2013.

[11] P. Lotfi, S. Soltani, and R. D. Murch, "Broadside beam-steerable planar parasitic pixel patch antenna," *IEEE Transactions on Antennas and Propagation*, vol. 64, no. 10, pp. 4519–4524, 2016.

[12] M. Hasan, I. Bahceci, M. A. Towfiq, T. M. Duman, and B. A. Cetiner, "Mode shift keying for reconfigurable mimo antennas: Performance analysis and antenna design," *IEEE Transactions on Vehicular Technology*, vol. 68, no. 1, pp. 320–334, 2019.

[13] A. Kalis, A. G. Kanatas, and C. B. Papadias, "A novel approach to mimo transmission using a single rf front end," *IEEE Journal on Selected Areas in Communications*, vol. 26, no. 6, pp. 972–980, 2008.

[14] A. Mohammadi and F. M. Ghannouchi, "Single rf front-end mimo transceivers," *IEEE Communications Magazine*, vol. 49, no. 12, pp. 104–109, 2011.

[15] A. K. Khandani, "Media-based modulation: A new approach to wireless transmission," in *2013 IEEE International Symposium on Information Theory*, 2013, pp. 3050–3054.

[16] A. K. Khandani and E. Bateni, "A practical, provably unbreakable approach to physical layer security," in *2019 16th Canadian Workshop on Information Theory (CWIT)*, 2019, pp. 1–6.

[17] A. K. Khandani, "Media-based modulation: Converting static rayleigh fading to awgn," in *2014 IEEE International Symposium on Information Theory*, 2014, pp. 1549–1553.

[18] E. Seifi, M. Atamanesh, and A. K. Khandani, "Media-based mimo: A new frontier in wireless communications," 2015.

[19] ——, "Media-based mimo: Outperforming known limits in wireless," in *2016 IEEE International Conference on Communications (ICC)*, 2016, pp. 1–7.

[20] C. L. Holloway, E. F. Kuester, J. A. Gordon, J. O'Hara, J. Booth, and D. R. Smith, "An overview of the theory and applications of metasurfaces: The two-dimensional equivalents of metamaterials," *IEEE Antennas and Propagation Magazine*, vol. 54, no. 2, pp. 10–35, 2012.

[21] H. Li, G. Wang, H.-X. Xu, T. Cai, and J. Liang, "X-band phase-gradient metasurface for high-gain lens antenna application," *IEEE Transactions on Antennas and Propagation*, vol. 63, no. 11, pp. 5144–5149, 2015.

[22] N. Nasimuddin, Z. N. Chen, and X. Qing, "Bandwidth enhancement of a single-feed circularly polarized antenna using a metasurface: Metamaterial-based wideband cp rectangular microstrip antenna." *IEEE Antennas and Propagation Magazine*, vol. 58, no. 2, pp. 39–46, 2016.

[23] C. P. Scarborough, D. H. Werner, and D. E. Wolfe, "Compact low-profile tunable metasurface-enabled antenna with near-arbitrary polarization," *IEEE Transactions on Antennas and Propagation*, vol. 64, no. 7, pp. 2775–2783, 2016.

[24] A. Forouzmand and H. Mosallaei, "Real-time controllable and multi-functional metasurfaces utilizing indium tin oxide materials: A phased array perspective," *IEEE Transactions on Nanotechnology*, vol. 16, no. 2, pp. 296–306, 2017.

[25] D. González-Ovejero, G. Minatti, G. Chattopadhyay, and S. Maci, "Multibeam by metasurface antennas," *IEEE Transactions on Antennas and Propagation*, vol. 65, no. 6, pp. 2923–2930, 2017.

[26] Y. Zhao, X. Cao, J. Gao, X. Yao, T. Liu, W. Li, and S. Li, "Broadband low-rcs metasurface and its application on antenna," *IEEE Transactions on Antennas and Propagation*, vol. 64, no. 7, pp. 2954–2962, 2016.

[27] A. Darvazehban, S. Ahdi Rezaeieh, A. Zamani, and A. M. Abbosh, "Pattern reconfigurable metasurface antenna for electromagnetic torso imaging," *IEEE Transactions on Antennas and Propagation*, vol. 67, no. 8, pp. 5453–5462, 2019.

[28] A. Dadgarpour, B. Zarghooni, B. S. Virdee, T. A. Denidni, and A. A. Kishk, "Mutual coupling reduction in dielectric resonator antennas using metasurface shield for 60-ghz mimo systems," *IEEE Antennas and Wireless Propagation Letters*, vol. 16, pp. 477–480, 2017.

[29] B. Feng, J. Lai, Q. Zeng, and K. L. Chung, "A dual-wideband and high gain magneto-electric dipole antenna and its 3d mimo system with metasurface for 5g/wimax/wlan/x-band applications," *IEEE Access*, vol. 6, pp. 33 387–33 398, 2018.

[30] T.-J. Cui, S. Liu, and L.-L. Li, "Information entropy of coding metasurface," *Light: Science & Applications*, vol. 5, no. 11, pp. e16 172–e16 172, Nov 2016. [Online]. Available: https://doi.org/10.1038/lsa.2016.172

[31] W. Tang, M. Z. Chen, J. Y. Dai, Y. Zeng, X. Zhao, S. Jin, Q. Cheng, and T. J. Cui, "Wireless communications with programmable metasurface: New paradigms, opportunities, and challenges on transceiver design," *IEEE Wireless Communications*, vol. 27, no. 2, pp. 180–187, 2020.

[32] L. Zhang, M. Z. Chen, W. Tang, J. Y. Dai, L. Miao, X. Y. Zhou, S. Jin, Q. Cheng, and T. J. Cui, "A wireless communication scheme based on space- and frequency-division multiplexing using digital metasurfaces," *Nature Electronics*, vol. 4, no. 3, pp. 218–227, Mar 2021. [Online]. Available: https://doi.org/10.1038/s41928-021-00554-4

[33] W. Tang, X. Li, J. Y. Dai, S. Jin, Y. Zeng, Q. Cheng, and T. J. Cui, "Wireless communications with programmable metasurface: Transceiver design and experimental results," *China Communications*, vol. 16, no. 5, pp. 46–61, 2019.

[34] W. Tang, J. Y. Dai, M. Chen, X. Li, Q. Cheng, S. Jin, K. Wong, and T. J. Cui, "Programmable metasurface-based rf chain-free 8psk wireless transmitter," *Electronics Letters*, vol. 55, no. 7, p. 417–420, Apr 2019. [Online]. Available: http://dx.doi.org/10.1049/el.2019.0400

[35] H. Zhao, Y. Shuang, M. Wei, T. J. Cui, P. d. Hougne, and L. Li, "Metasurface-assisted massive backscatter wireless communication with commodity wi-fi signals," *Nature Communications*, vol. 11, no. 1, p. 3926, Aug 2020. [Online]. Available: https://doi.org/10.1038/s41467-020-17808-y

[36] E. Basar, M. Di Renzo, J. De Rosny, M. Debbah, M.-S. Alouini, and R. Zhang, "Wireless communications through reconfigurable intelligent surfaces," *IEEE Access*, vol. 7, pp. 116 753–116 773, 2019.

[37] J. Zhao, "A survey of intelligent reflecting surfaces (irss): Towards 6g wireless communication networks," 2019.

[38] K. J. Vinoy, A. Chockalingam, A. Roy, P. Ashwin, Y. Naresh, A. Venkatarmana, and S. Roy, "A digitally reconfigurable meta-surface for communication in scatter-rich multipath channel," Indian Patent 202 141 039 005, Aug. 27, 2021.

[39] A. Roy and K. J. Vinoy, "A reconfigurable array for media based spatial modulation," in *2019 49th European Microwave Conference (EuMC)*, 2019, pp. 880–883.

[40] K. Kawabe, H. Koyama, and K. Shirae, "Planar inductor," *IEEE Transactions on Magnetics*, vol. 20, no. 5, pp. 1804–1806, 1984.

[41] A. Shlykevich, T. Bystricky, and T. Blecha, "High frequency properties of rf planar passive components," *Periodica Polytechnica Electrical Engineering and Computer Science*, vol. 61, no. 1, pp. 48–53, 2017. [Online]. Available: https://pp.bme.hu/eecs/article/view/9734

[42] A. Roy and K. J. Vinoy, "A reconfigurable screen in the antenna nearfield for media-based modulation scheme," in *2018 IEEE MTT-S International Microwave and RF Conference (IMaRC)*, 2018, pp. 1–4.

[43] D. Rodrigo, B. A. Cetiner, and L. Jofre, "Frequency, radiation pattern and polarization reconfigurable antenna using a parasitic pixel layer," *IEEE Transactions on Antennas and Propagation*, vol. 62, no. 6, pp. 3422–3427, 2014.

[44] A. Roy, P. Ashwin, K. J. Vinoy, and A. Chockalingam. (2021, Aug.) Data Transfer with Channel Alphabets using a Switchable Metasurface-MicrowaveLab-ECE-IISc. [Online]. Available: https://www.youtube.com/watch?v=xLOb8m0Ku70